

CALCULATION OF MINIMUM CRITICAL REYNOLDS NUMBER FOR LAMINAR-TURBULENT TRANSITION IN PIPE FLOWS*

HIDESADA KANDA[†]

Abstract. This article describes the calculation of the minimum critical Reynolds number for laminar-turbulent transition in pipe flows. From the conclusions of our previous experimental study, it is clear that a transition occurs near the pipe inlet and the critical Reynolds number R_c takes the minimum value of about 2000 in the case of a straight pipe. Moreover, in our previous calculations of laminar entrance pipe flow, it was found that near the pipe inlet a large pressure gradient in the radial direction exists, which decreases as the Reynolds number Re increases. Thus, we have built a new transition macromodel to determine R_c using the effect of the radial pressure gradient. The calculated results were $R_c(min) = 3750$ when the number of radial grid points $J_0 = 51$ and 2200 when $J_0 = 101$.

Key words. hydrodynamic stability, grid refinement, thermodynamics

AMS subject classifications. 76E05, 65M50, 80A05

1. Introduction and summary. Osborne Reynolds found two critical Reynolds numbers (R_c) in pipe flows: R_{c1} of 12,830 from laminar to turbulent flow and R_{c2} of 2030 from turbulent to laminar flow [16]. Ever since the pioneering experimental work of Reynolds (1883), the issue of how and why the fluid flow along a circular pipe changes from being laminar to turbulent as the flow rate increases has intrigued physicists, mathematicians, and engineers alike [11].

The objectives of this investigation are to derive a macromodel of laminar-turbulent transition for Hagen-Poiseuille flow or pipe flow and to calculate the minimum value of the critical Reynolds number $R_c(min)$, which is in the neighborhood of 2000.

To date, attempts to theoretically obtain values of R_c have been undertaken using stability theory with the Orr-Sommerfeld equation and disturbances. However, $R_c(min)$ of approximately 2000 has not yet been calculated. For flow in the entrance region, Tatsumi obtained $R_c = 19,400$ [21], and Huang and Chen obtained $R_c = 39,800$ and 39,560 with axisymmetric and non-axisymmetric disturbances, respectively [5, 6]. In the fully developed region, the flow is stable with respect to both axisymmetric and non-axisymmetric disturbances [2]. In this study, we do not further consider such stability theory.

The line of thought on calculating R_c for laminar-turbulent transition is formulated on the basis of our experiments [10] and calculated results [8, 9].

(1) The Reynolds number (Re) primarily and generally affects R_c , since transition occurs as Re increases. Therefore, we must further study what factor, besides Re , mainly affects R_c .

(2) The laminar-turbulent transition occurs near the pipe inlet in the entrance region. It is important to note that the flow may become turbulent long before it becomes fully developed [4, 20].

(3) We must numerically find a new unknown variable which varies near the inlet. It is the normal wall strength (NWS); see Subsection 3.1.

(4) We must numerically evaluate the effects of NWS on R_c in this study.

First, from the viewpoint of our experiments, let us consider the problem in more detail.

(5) R_c is apparently determined by the entrance shape or the contraction ratio $C_b (= D_b/D)$ of the bellmouth diameter D_b to pipe diameter D . In most previous experi-

*Received January 10, 2008. Accepted for publication March 19, 2008. Published online on July 23, 2008. Recommended by F. Stenger.

[†]Computer Science and Engineering, University of Aizu, Aizu-Wakamatsu, Fukushima 965-8580, Japan (kanda@u-aizu.ac.jp).

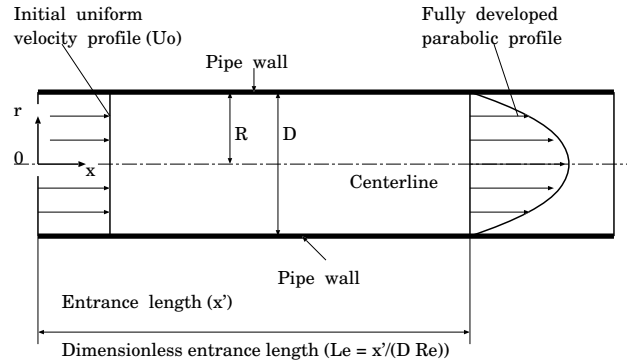


FIG. 1.1. Velocity development in entrance region of a straight circular pipe.

ments, pipes were fitted with trumpet mouthpieces or bellmouths at the inlet, so that water might enter without disturbances. $R_c(min)$ of approximately 2000 is obtained in the case of a straight circular pipe. The sharp edge of the straight pipe is not a singular point in the transition, since R_c is a smooth function of C_b at ≈ 2000 .

(6) The transition occurs near the pipe inlet. For example, in the case of a straight pipe, the transition occurs approximately 6–13 diameters downstream at $Re \approx 2000$. Consider a dimensionless axial coordinate (X); let x' be the actual axial coordinate, then $X = x'/(DRe)$. For the above example, the transition occurs at the pipe inlet of $X \leq 13/2000 = 0.0065$.

(7) For Reynolds' color-band experiments, R_c varies when $C_b = 1-2.3$, particularly when $C_b = 1-1.4$. If the radial distance of $C_b = 1.4$ is transformed to the axial distance to check the order of length, then for $Re \approx 2000$, $X \leq 1.4/2000 = 0.0007$.

Second, let us consider the viewpoint of previous experimental and numerical results. In the entrance region, the velocity profile changes from a uniform distribution at the pipe inlet to a parabolic one at the entrance length, as shown in Fig. 1.1. Generally, thus far, three major variables have been studied [3]: (i) the velocity distribution in all sections, (ii) the entrance length L_e , which is defined as the distance from the inlet to the point where the centerline velocity reaches 99% of the fully developed value, and (iii) the pressure drop Δp . The region from the inlet to L_e is called the entrance region and the downstream region from L_e is called the fully developed region.

L_e [1] is expressed as

$$(1.1) \quad Le = \frac{x'}{DRe} = \frac{0.60}{Re(0.035Re + 1)} + 0.056.$$

From (1.1), $Le = 0.0562$ at $Re = 300$, and Le takes a constant value of 0.056 at $Re \geq 500$. The total pressure drop $\Delta p(X)$ from the pipe inlet is expressed as the sum of the pressure drop $64X$ that would occur if the flow were fully developed, plus the excess pressure drop $K(X)$ to account for the developing region.

$$\Delta p(X) = p(0) - p(X) = -p(X) = 64X + K(X)$$

$K(X)$ is assumed to be $K(\infty)$ in (1.2) for the fully developed region [1]. From (1.2), $K(\infty)$ is 1.276 at $Re = 500$ and 1.219 at $Re = 2000$. $K(\infty)$ is approximately the same at $Re \geq 500$.

$$(1.2) \quad K(\infty) = 1.20 + \frac{38}{Re}$$

(8) We discuss properties (a) and (b) of two parameters, which will enable us to determine accurate values of R_c : parameter (a) is a constant regardless of Re for $Re \geq 500$ while parameter (b) varies inversely as Re increases. The intersection of the lines of the parameters should indicate a critical value; see Fig. 4.3.

(9) It is clear from (1.1) that the velocity distribution and L_e in the X coordinate are approximately the same at $Re \geq 500$. Thus, parameter (a) of a constant magnitude is set to be the increase in kinetic energy KE on the basis of the velocity development from a uniform to a parabolic profile; see Subsection 3.3. Concerning moving fluid particles, the physical unit of KE is power, i.e., energy per second.

(10) We found numerically that at $Re \approx R_c$, a large pressure gradient exists in the normal direction near the inlet and disappears as Re increases. This normal pressure gradient is caused by NWS.

(11) We must evaluate the relationship between R_c and the normal pressure gradient or NWS. The first law of thermodynamics (conservation of energy) states that the increase in the energy of a material region is the result of work and heat transfers to the region [12]. If there is no heat transfer, then some work is done on the fluid particles for KE. The physical units of energy and work are the same. Thus, parameter (b) is set to be the power RW done by NWS.

Therefore, the main research subject is to numerically investigate the relationship among KE, RW, and R_c .

2. Calculation of radial pressure gradient.

2.1. Governing equations. First, we consider dimensionless variables. All lengths and velocities are normalized by the pipe diameter D and the mean velocity U_0 , respectively. The pressure is normalized by $(1/2)\rho U_0^2$. Re is based on U_0 and D . Note that the dimensionless axial coordinate $x (= x'/D)$ is used for calculation and $X (= x'/(DRe))$ is used in our figures and tables, where x' is the actual axial coordinate.

We consider unsteady flow of an incompressible Newtonian fluid with a constant viscosity and density, and we disregard gravity and external forces. We introduce the streamfunction and vorticity formulas in the two-dimensional cylindrical coordinates for the governing equations in order to avoid the explicit appearance of the pressure term. Accordingly, the velocity fields are determined without any assumptions concerning the pressure. Subsequently, the pressure distribution is calculated using the values of the velocity fields.

The dimensionless transport equation for the vorticity is expressed as

$$(2.1) \quad \frac{\partial \omega}{\partial t} - \frac{1}{r} \frac{\partial \psi}{\partial x} \frac{\partial \omega}{\partial r} + \frac{1}{r} \frac{\partial \psi}{\partial r} \frac{\partial \omega}{\partial x} + \frac{\omega}{r^2} \frac{\partial \psi}{\partial x} = \frac{1}{Re} \left\{ \frac{\partial}{\partial r} \left[\frac{1}{r} \frac{\partial (r\omega)}{\partial r} \right] + \frac{\partial^2 \omega}{\partial x^2} \right\}.$$

The Poisson equation for ω is derived from the definition of ω , i.e.,

$$(2.2) \quad -\omega = \nabla^2 \psi = \frac{\partial}{\partial r} \left(\frac{1}{r} \frac{\partial \psi}{\partial r} \right) + \frac{\partial^2 \psi}{\partial x^2}.$$

The axial velocity u and radial velocity v are defined as the derivatives of the streamfunction, i.e.,

$$(2.3) \quad u = \frac{1}{r} \frac{\partial \psi}{\partial r}, \quad v = -\frac{1}{r} \frac{\partial \psi}{\partial x}.$$

Only the angular (θ) component of a two-dimensional flow field ω is non-negligible; thus, we shall replace ω_θ with ω ,

$$(2.4) \quad \omega = \omega_\theta = [\nabla \times V]_\theta = \frac{\partial v}{\partial x} - \frac{\partial u}{\partial r}.$$

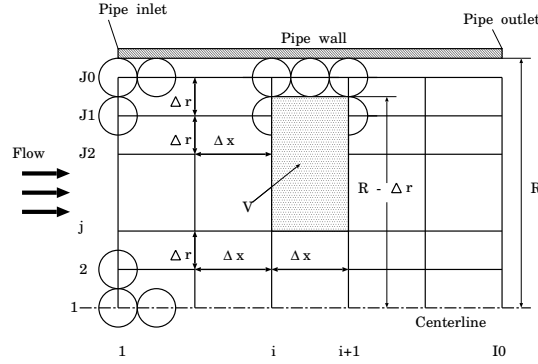


FIG. 2.1. Grid system in a circular straight pipe.

The pressure can be calculated using the steady-state form of the Navier-Stokes (N-S) equations. The pressure distribution for the x derivative is

$$(2.5) \quad \frac{\partial p}{\partial x} = -2 \left(u \frac{\partial u}{\partial x} + v \frac{\partial u}{\partial r} \right) + \frac{2}{\text{Re}} \left(\frac{\partial^2 u}{\partial x^2} + \frac{1}{r} \frac{\partial u}{\partial r} + \frac{\partial^2 u}{\partial r^2} \right),$$

and that for the r derivative is

$$(2.6) \quad \frac{\partial p}{\partial r} = -2 \left(u \frac{\partial v}{\partial x} + v \frac{\partial v}{\partial r} \right) + \frac{2}{\text{Re}} \left(\frac{\partial^2 v}{\partial x^2} + \frac{1}{r} \frac{\partial v}{\partial r} - \frac{v}{r^2} + \frac{\partial^2 v}{\partial r^2} \right).$$

Since u and v are known at every point, from (2.3), a smooth pressure distribution that satisfies both (2.5) and (2.6) is calculated using Poisson's equation (2.7) [15],

$$(2.7) \quad \nabla^2 p = \frac{\partial^2 p}{\partial x^2} + \frac{\partial^2 p}{\partial r^2} + \frac{1}{r} \frac{\partial p}{\partial r} = -2 \left[\left(\frac{\partial v}{\partial r} \right)^2 + 2 \frac{\partial u}{\partial r} \frac{\partial v}{\partial x} + \left(\frac{\partial u}{\partial x} \right)^2 + \frac{v^2}{r^2} \right].$$

In this study, initial values are obtained using (2.5), and then (2.7) is used to obtain better solutions.

2.2. Numerical method for vorticity transport equation. The rectangular grid system used here is schematically illustrated in Fig. 2.1, where $I0$ and $J0$ are the maximum numbers for axial and radial grid points, respectively, and $I1 = I0 - 1$, $I2 = I0 - 2$, $J1 = J0 - 1$, and $J2 = J0 - 2$.

To obtain precise results in this study, we used a refined axial grid of $\Delta X = 0.00001$. For calculations, the dimensionless axial grid $\Delta x (= \Delta X \times \text{Re})$ is used. The grid space $\Delta x' (= \Delta X \times D \times \text{Re})$ in actual length is considered. For a pipe of $D = 2.6$ cm and $\text{Re} = 2000$, the dimensionless grid space $\Delta X = 0.00001$ corresponds to $\Delta x' = 0.052$ cm in actual length: $\Delta x' = 0.00001 \times 2.6 \times 2000 = 0.052$; for $\text{Re} = 10,000$, $\Delta X = 0.00001$ corresponds to $\Delta x' = 0.26$ cm in actual length. Two grid systems are used: (i) $I0 = 1001$, $J0 = 51$, and $\Delta X = 0.00001$, and (ii) $J0 = 101$. The maximum X is 0.01.

For unsteady problems, generally, an explicit method is faster than an implicit method in CPU time, but lacks calculation stability. The finite difference equation for (2.1) was first solved by the Gauss-Seidel explicit iterative method [7, 8, 9], where calculation stability was achieved by adding steps 4–5 in Fig. A.1; see Appendix. This explicit scheme, however, required long CPU times to maintain computational stability. Next, it was improved by the

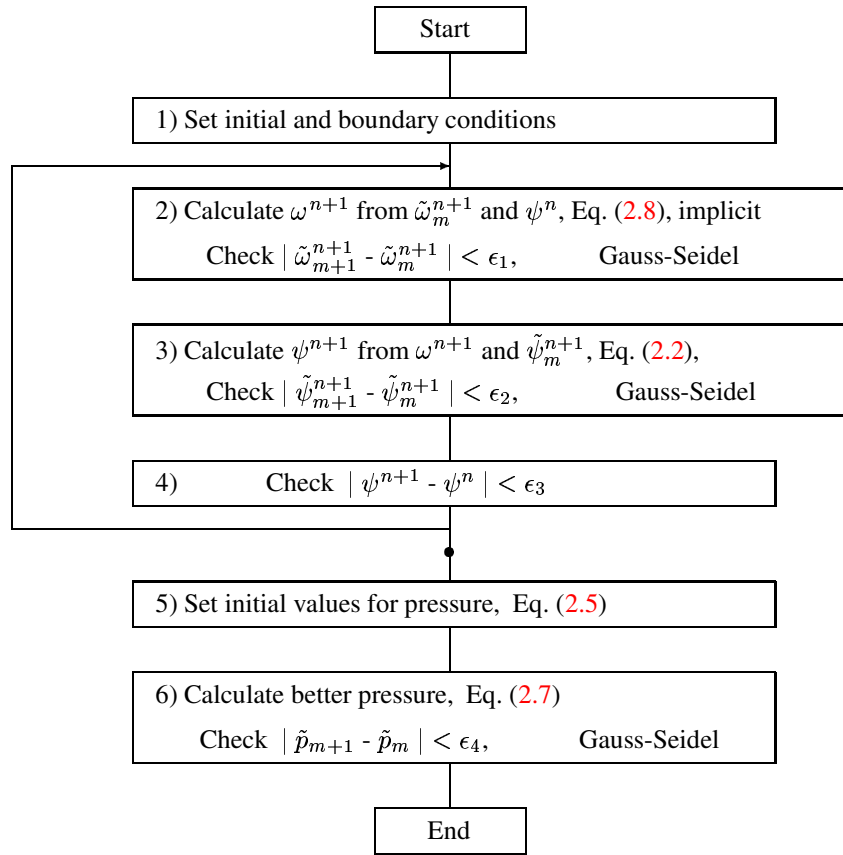


FIG. 2.2. Flowchart for implicit iteration method.

implicit method shown in Fig. 2.2, where $\tilde{\omega}$ and $\tilde{\psi}$ are provisional values, n is the time step, and m is the index of iteration [18, 19]. In this study, we use the implicit method.

The implicit form for (2.1) is written as

$$(2.8) \quad \frac{\omega^{n+1} - \omega^n}{\Delta t} - \frac{1}{r} \frac{\partial \psi^n}{\partial x} \frac{\partial \omega^{n+1}}{\partial r} + \frac{1}{r} \frac{\partial \psi^n}{\partial r} \frac{\partial \omega^{n+1}}{\partial x} + \frac{\omega^{n+1}}{r^2} \frac{\partial \psi^n}{\partial x} = \frac{1}{\text{Re}} \left\{ \frac{\partial}{\partial r} \left[\frac{1}{r} \frac{\partial (r \omega^{n+1})}{\partial r} \right] + \frac{\partial^2 \omega^{n+1}}{\partial x^2} \right\}.$$

This computational scheme involves the Forward-Time, Centered-Space (FTCS) method. At the wall, a three-point, one-sided approximation for derivatives is used to maintain second-order accuracy. The scheme thus has second-order accuracy in space variables and first-order accuracy in time.

Consider the initial streamfunction. From (2.3), the initial condition for the streamfunction is given by

$$\psi(i, j) = \frac{1}{2}[(j-1)\Delta r]^2, \quad 1 \leq i \leq I0, \quad 1 \leq j \leq J0.$$

Within the boundaries, the initial vorticity is obtained by solving (2.2). The velocities u and v are set using (2.3) whenever the streamfunction is newly calculated.

The following are the boundary conditions.

- (i) At the centerline: $\psi_{i,1} = 0$, $\omega_{i,1} = 0$, $1 \leq i \leq I1$.
- (ii) At the inlet: $\psi_{1,j} = 0.5[(j-1)\Delta r]^2$, $\omega_{1,j} = 0$, $2 \leq j \leq J1$.
- (iii) At the wall: $\psi_{i,J0} = 0.5[(J0-1)\Delta r]^2$, $1 \leq i \leq I1$.

The vorticity boundary condition at the no-slip walls is derived from (2.4) as

$$(2.9) \quad \omega = -\frac{\partial u}{\partial r}.$$

A three-point, one-sided approximation for (2.9) is used to maintain second-order accuracy,

$$(2.10) \quad \omega_{i,J0} \approx -\frac{3u_{i,J0} - 4u_{i,J1} + u_{i,J2}}{2\Delta r} = \frac{4u_{i,J1} - u_{i,J2}}{2\Delta r}.$$

- (iv) At the outlet, the linear extrapolation method is used: $\psi_{I0,j} = 2\psi_{I1,j} - \psi_{I2,j}$, $\omega_{I0,j} = 2\omega_{I1,j} - \omega_{I2,j}$, $1 \leq j \leq J0$.

The following are the boundary conditions for pressure.

- (v) For the pressure at the centerline, we use the three-point finite difference form. Since $\partial p / \partial r = 0$ at $r = 0$,

$$p_{i,1} = \frac{4p_{i,2} - p_{i,3}}{3}, \quad 1 \leq i \leq I0.$$

- (vi) The pressure at the inlet is given as zero without the leading edge: $p_{1,j} = 0$, $1 \leq j \leq J1$.

- (vii) The pressure at the wall is derived from (3.2); see Subsection 3.1. For the leading edge with $i = 1$ and $j = J0$, the three-point approximation is used for p and ω , and the pressure gradient is expressed as

$$\left. \frac{\partial p}{\partial r} \right|_{i=1, j=J0} \approx \frac{3p_{1,J0} - 4p_{1,J1} + p_{1,J2}}{2\Delta r} = \frac{2}{\text{Re}} \left(\frac{-\omega_{3,J0} + 4\omega_{2,J0} - 3\omega_{1,J0}}{2\Delta x} \right).$$

For the wall with $2 \leq i \leq I1$ and $J = J0$,

$$\left. \frac{\partial p}{\partial r} \right|_{i \geq 2, j=J0} \approx \frac{3p_{i,J0} - 4p_{i,J1} + p_{i,J2}}{2\Delta r} = \frac{2}{\text{Re}} \left(\frac{\omega_{i+1,J0} - \omega_{i-1,J0}}{2\Delta x} \right).$$

- (viii) For the outflow boundary conditions, the linear extrapolation method is used: $p_{I0,j} = 2p_{I1,j} - p_{I2,j}$, $1 \leq j \leq J0$.

2.3. Calculated results of radial pressure gradient. The numerical calculations were carried out for $\text{Re} = 500, 1000, 2000, 3000, 5000$, and $10,000$ in 2006 on an NEC SX-7 supercomputer with a peak performance of 8.83G-FLOPS/processor. Table 2.1 lists Re , grid systems, time step (Δt), number of time steps until steady state (T-steps), and CPU times. Δt was 0.0001 from T-step = 0 to 100,000, and was increased to 0.0002 or gradually to 0.0002, 0.0003, and 0.0005.

Figures 2.3 through 2.7 show the calculated results of (a) axial pressure drop and (b) pressure distribution in the radial direction. The relationship between the pressure (p) and pressure drop (Δp) is $\Delta p = 0 - p = -p$, where p is zero at the inlet.

To verify the accuracy of calculations, the results of calculations are compared with the smooth curves drawn using Shapiro et al.'s experimental results [17], as shown in Fig. 2.3(a)

TABLE 2.1
 Grid system, time step Δt , T-steps, and CPU times.

Re	I0/J0	Δt	T-steps	CPU
500	1000/51	0.0001–0.0005	6,000,000	10h 42m
1000	1000/51	0.0001–0.0002	9,000,000	20h 26m
2000	1000/51	0.0001–0.0002	9,000,000	22h 34m
3000	1000/51	0.0001–0.0002	9,000,000	27h 13m
5000	1000/51	0.0001–0.0005	6,000,000	10h 17m
10,000	1000/51	0.0001–0.0005	6,000,000	11h 24m
500	1000/101	0.0001–0.0005	6,000,000	24h 54m
1000	1000/101	0.0001–0.0002	8,000,000	26h 27m
2000	1000/101	0.0001–0.0002	9,000,000	31h 06m
3000	1000/101	0.0001–0.0002	10,000,000	30h 30m
5000	1000/101	0.0001–0.0002	10,000,000	49h 39m
10,000	1000/101	0.0001–0.0002	10,000,000	30h 59m

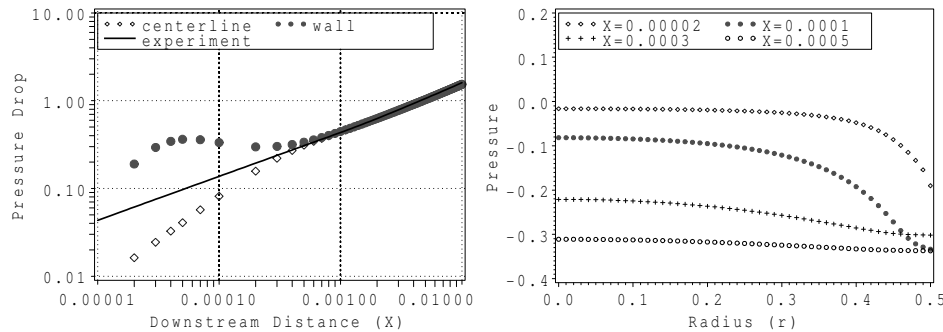


FIG. 2.3. (a) Axial pressure drop and (b) pressure distribution in r -direction, $Re = 1000$.

through 2.7(a), where the diamond and dot symbols denote the calculated results for pressure at the centerline (p_c) and for pressure at the wall (p_w), respectively. Near the pipe inlet, the experimental results fall between p_c and p_w and agree well with the computed results downstream.

The major conclusions concerning the radial pressure distribution are as follows. Here, $(\Delta p_w - \Delta p_c) = (p_c - p_w)$.

(1) It is clear, from Fig. 2.3(a), that at $Re = 1000$, there is a large difference between Δp_w and Δp_c across the radius of the pipe at $X < 0.0003$, and that this difference decreases as X increases.

(2) It is seen, from Figs. 2.3(a) through 2.7(a), that the difference $(\Delta p_w - \Delta p_c)$ decreases as Re increases. At $Re = 10,000$, the difference exists at $X < 0.00005$ and disappears downstream.

(3) Note that Δp_w is larger than Δp_c . This indicates that p_w is lower than p_c , as verified in Figs. 2.3(b) through 2.7(b). This difference contradicts the results obtained by others using the boundary-layer theory, and it also contradicts Bernoulli’s law, although Bernoulli’s law does not apply to viscous flow. The radial pressure gradient $\partial p / \partial r$ near the wall and inlet is seen to be large, but it decreases near the centerline and downstream.

2.4. Radial pressure distribution. Let us consider the question theoretically: “Which is higher, p_w or p_c in the radial direction?” Since the axial velocity $u_{i,j0}$ is zero at the wall,

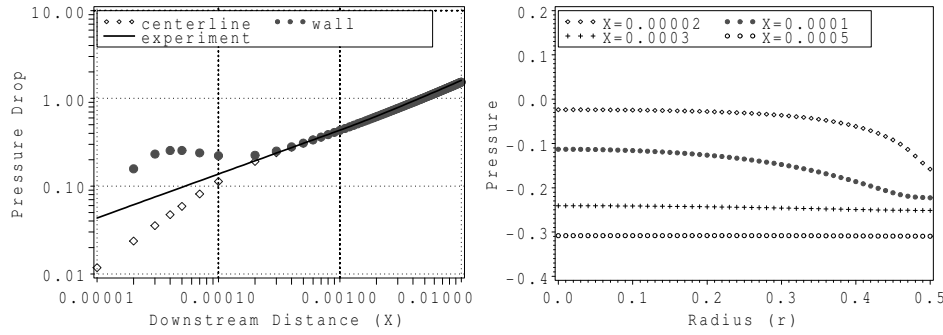


FIG. 2.4. (a) Axial pressure drop and (b) pressure distribution in r -direction, $Re = 2000$.

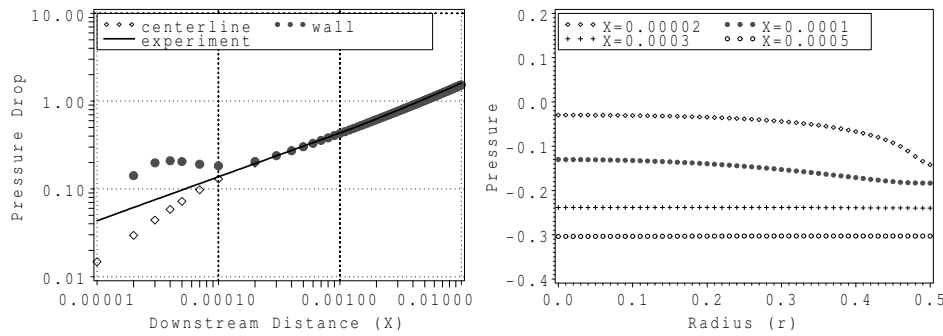


FIG. 2.5. (a) Axial pressure drop and (b) pressure distribution in r -direction, $Re = 3000$.

the x component of velocity, u , can be linearly approximated as

$$(2.11) \quad u_{i,J1} \approx \frac{(u_{i,J0} + u_{i,J2})}{2} = \frac{1}{2}u_{i,J2}.$$

From (2.9), (2.10), and (2.11), the vorticity at the wall is simply approximated as

$$(2.12) \quad \omega_{i,J0} = - \left. \frac{\partial u}{\partial r} \right|_{r=R} \approx \frac{u_{i,J1}}{\Delta r} > 0.$$

Substituting (2.12) into (3.2) (see Subsection 3.1) gives

$$(2.13) \quad \begin{aligned} \left. \frac{\partial p}{\partial r} \right|_{r=R} &= \frac{2}{Re} \left. \frac{\partial \omega_\theta}{\partial x} \right|_{r=R} \approx \frac{2}{Re} \frac{\partial}{\partial x} \left(\frac{u_{i,J1}}{\Delta r} \right) \\ &\approx \frac{2}{Re} \left(\frac{u_{i+1,J1} - u_{i-1,J1}}{2\Delta x \Delta r} \right) \leq 0. \end{aligned}$$

Thus, since $u_{i+1,J1} < u_{i-1,J1}$ in the entrance region, the normal pressure gradient at the wall becomes negative. Therefore, it is verified from (2.13) that the pressure gradient in the radial direction is negative at the wall of the entrance region.

On the other hand, in the fully developed region, since $u_{i+1,J1} = u_{i-1,J1}$ in (2.13), the normal pressure gradient at the wall becomes 0, thus making the pressure distribution uniform in the radial direction.

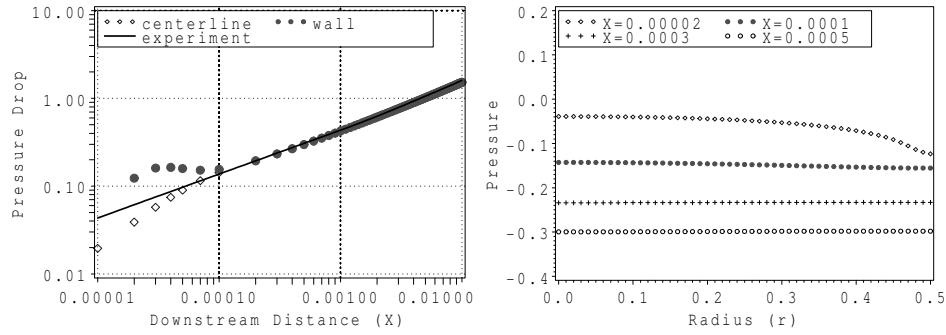


FIG. 2.6. (a) Axial pressure drop and (b) pressure distribution in r -direction, $Re = 5000$.

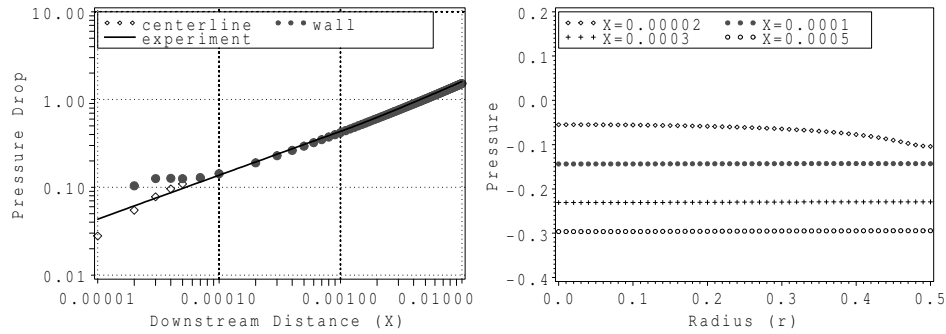


FIG. 2.7. (a) Axial pressure drop and (b) pressure distribution in r -direction, $Re = 10,000$.

The velocity distribution in the fully developed region is given by

$$(2.14) \quad u(r) = 2U_0 \left[1 - \left(\frac{r}{R} \right)^2 \right],$$

where $U_0 = 1$ in dimensionless form. Differentiating (2.14) with respect to r gives

$$\omega|_{r=R} = - \left. \frac{\partial u}{\partial r} \right|_{r=R} = -2 \left(-\frac{2R}{R^2} \right) = 4 \frac{1}{R} = 8,$$

where the dimensionless value of R is 0.5. Thus, the value of ω monotonically decreases from a large positive value at the leading edge to 8 in the fully developed region.

3. Evaluation of radial pressure gradient.

3.1. Normal pressure gradient at wall. Here, we consider the radial pressure gradient $\partial p / \partial r$. The dimensionless N-S equation in vector form [3] is written as

$$(3.1) \quad \frac{\partial V}{\partial t} - V \times \omega = -\frac{1}{2} \text{grad} (p + V^2) - \frac{1}{Re} \nabla \times \omega.$$

Since the velocity vector $V = 0$ at the wall, the normal component of (3.1) at the wall reduces to

$$(3.2) \quad \left. \frac{\partial p}{\partial r} \right|_{r=R} = -\frac{2}{Re} \nabla \times \omega|_{r=R} = \frac{2}{Re} \left. \frac{\partial \omega_\theta}{\partial x} \right|_{r=R}.$$

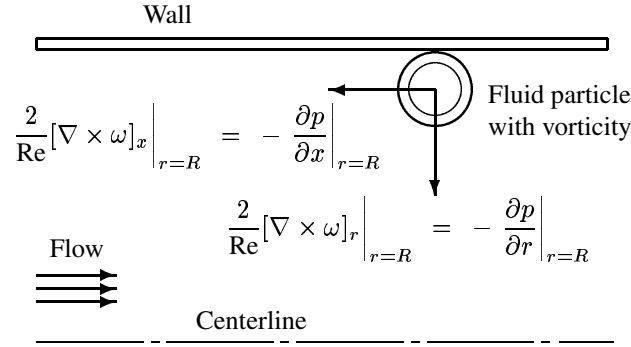


FIG. 3.1. Directions of curl of vorticity at wall.

Note that the normal pressure gradient is derived from the negative normal component of the curl of vorticity at the wall, which is hereafter called the normal wall strength NWS. From (3.2), NWS is expressed as

$$(3.3) \quad \text{NWS} \equiv \frac{2}{\text{Re}} \nabla \times \omega|_{r=R} = - \frac{2}{\text{Re}} \frac{\partial \omega_\theta}{\partial x} \Big|_{r=R} = - \frac{\partial p}{\partial r} \Big|_{r=R}.$$

The following characteristics of NWS are considered.

(i) NWS is effective near the pipe inlet, where the vorticity gradient in the x -direction is large and decreases inversely with Re . In the fully developed region, NWS vanishes since the vorticity at the wall is constant and then the curl of vorticity disappears.

(ii) It is clear from (3.3) that NWS causes a pressure gradient in the radial direction, that is, the pressure gradient at the wall results from the curl of vorticity. NWS and the radial pressure gradient $\partial p/\partial r$ have the same magnitude at the wall, but are opposite in direction. When $\partial p/\partial r < 0$, NWS is directed from the wall to the centerline, as shown in Fig. 3.1. Note that NWS causes the fluid particles near the wall to move towards the centerline in the normal direction, i.e., it accelerates the fluid particles in the central core.

(iii) When adopting the boundary-layer assumption, NWS vanishes since $\partial p/\partial r$ is always neglected in the assumption.

3.2. Tangential-vorticity source strength. We consider other forces at the wall in accordance with Lighthill [13]. Vorticity is produced on a solid body or solid wall surface and spreads from there into the fluid. At almost all points on the boundary, the vorticity has a nonzero gradient along the normal. This gradient, multiplied by $(2/\text{Re})$, represents the flow of total vorticity out of the surface per unit area per unit time, so that it is the local strength of the surface distribution of vorticity sources.

(1) Tangential-vorticity source strength.

The tangential-vorticity source strength has a simple relationship with pressure gradient. If the surface is taken as $r = R$, the flow of θ -vorticity out of it is expressed as

$$- \frac{2}{\text{Re}} \left[\frac{1}{r} \frac{\partial(r\omega)}{\partial r} \right] = \frac{2}{\text{Re}} \left[\frac{1}{r} \frac{\partial}{\partial r} \left(r \frac{\partial u}{\partial r} \right) \right] = \frac{2}{\text{Re}} \nabla^2 u = - \frac{2}{\text{Re}} [\nabla \times \omega]_x = \frac{\partial p}{\partial x}.$$

Hence the tangential-vorticity source strength at the wall is identical to the axial component of the curl of vorticity multiplied by $(2/\text{Re})$ in magnitude, but opposite in direction, as shown in Fig. 3.1. Note that this strength affects the pressure gradient in the x -direction, but does not affect the pressure gradient in the normal or radial direction.

(2) Normal-vorticity source strength.

The normal-vorticity source strength is directly derived under the continuity condition on ω . The continuity equation for ω in cylindrical coordinates is

$$\operatorname{div} \omega \equiv \frac{1}{r} \frac{\partial(r\omega_r)}{\partial r} + \frac{1}{r} \frac{\partial\omega_\theta}{\partial \theta} + \frac{\partial\omega_z}{\partial z} = 0.$$

From the above equation, the normal-vorticity source strength is expressed as

$$\frac{2}{\operatorname{Re}} \frac{\partial}{\partial r}(r\omega_r) = - \frac{2}{\operatorname{Re}} \left[\frac{1}{r} \frac{\partial\omega_\theta}{\partial \theta} + \frac{\partial\omega_x}{\partial x} \right].$$

In two dimensions, ω_r , ω_x , and their derivative with respect to θ are all zero. Accordingly, this normal-vorticity source strength vanishes in the two-dimensional coordinates and affects nothing.

3.3. Increase in kinetic energy. In the entrance region, the velocity distribution changes from uniform at the inlet to parabolic in the fully developed region. The magnitude of the increase in kinetic energy is considered below.

(i) At the inlet, the velocity profile is uniform: $u(0, r) = U_0$. The kinetic energy across the inlet is given by multiplying the flux by its kinetic energy,

$$(3.4) \quad \int_0^R 2\pi r dr \cdot U_0 \cdot \left(\frac{1}{2}\rho U_0^2\right) = \frac{1}{8}\pi\rho D^2 U_0^3.$$

(ii) In the fully developed region, the velocity has a parabolic distribution (2.14). Accordingly, the kinetic energy is calculated as

$$(3.5) \quad \int_0^R 2\pi r \left(\frac{1}{2}\rho\right) \left\{ 2U_0 \left[1 - \left(\frac{r}{R}\right)^2 \right] \right\}^3 dr = \frac{1}{4}\pi\rho D^2 U_0^3.$$

(iii) The increase in kinetic energy (KE') in the entrance region is obtained by subtracting (3.4) from (3.5), which gives

$$\operatorname{KE}' = \frac{1}{4}\pi\rho D^2 U_0^3 - \frac{1}{8}\pi\rho D^2 U_0^3 = \frac{1}{8}\pi\rho D^2 U_0^3.$$

The dimension of this increase in kinetic energy is

$$\left[\frac{kg}{m^3} m^2 \left(\frac{m}{s}\right)^3 = kg \frac{m^2}{s^3} = kg \frac{m}{s^2} \frac{m}{s} \right].$$

This unit corresponds to physical power, i.e., energy per second. We define a dimensionless increase in kinetic energy per second, KE, as

$$(3.6) \quad \operatorname{KE} \equiv \frac{\frac{1}{8}\pi\rho D^2 U_0^3}{\frac{1}{2}\rho D^2 U_0^3} = \frac{\pi}{4} = 0.785.$$

This value of $\operatorname{KE} = 0.785$ is a constant and is independent of Re ; thus, KE satisfies the necessary condition of parameter (a). RW is similarly normalized by $(1/2)\rho D^2 U_0^3$; see Subsection 4.2.

4. Power done by NWS.

4.1. Variation of enthalpy with pressure. Using the pressure drop ($p_e - p_w$) in the radial direction, the amount of work WK done by NWS is considered. Here, on the basis of thermodynamics [12], the variation of enthalpy H with pressure p , at a fixed temperature, can be obtained from the definition $H = U + pV$, where U is the internal energy and V is the volume. For changes in H , we have

$$\Delta H = \Delta U + \Delta(pV).$$

For most solids and liquids, at a constant temperature, the internal energy $U(T, V)$ does not change as

$$dU = \left(\frac{\partial U}{\partial T} \right)_V dT + \left(\frac{\partial U}{\partial V} \right)_T dV = 0,$$

where T is the temperature. Since the change in volume is rather small, unless the changes in pressure are very large, the change in enthalpy ΔH resulting from a change in pressure Δp can be approximated by

$$(4.1) \quad \text{WK} = \Delta H \approx V \Delta p.$$

Equation (4.1) can be applied to incompressible flow as well. The unit of $V \Delta p$ is expressed as

$$\left[m^3 \cdot kg \frac{m}{s^2} \frac{1}{m^2} = kg \frac{m^2}{s^2} = kg \frac{m}{s^2} \cdot m \right].$$

This unit, however, is equal to work in physics, and not to power such as KE.

4.2. Power done by NWS. The power RW done by NWS, or the rate of change of the work WK, can be obtained by dividing the work given in (4.1) by period Δt , but at this point, the period is not yet known,

$$\text{RW} = \frac{\text{WK}}{\Delta t} = \frac{V \Delta p}{\Delta t}.$$

Here, consider the dimensionless RW. RW is normalized by the same method as KE in (3.6). Lengths, pressure, and time are normalized by D , $(1/2)\rho U_0^2$, and (D/U_0) , respectively. Accordingly, the dimensionless RW is expressed as

$$\text{RW} = \frac{V \Delta p}{\Delta t} = \frac{\frac{V' \Delta p'}{\Delta t'}}{D^3 \cdot (1/2)\rho U_0^2 \cdot (U_0/D)} = \frac{\frac{V' \Delta p'}{\Delta t'}}{(1/2)\rho D^2 U_0^3},$$

where $(')$ denotes dimensional quantities.

The power RW will be determined by the following steps.

(1) We begin by calculating the work from (4.1) for the shaded space between $x(i)$ and $x(i+1)$ in Fig. 2.1, where it is assumed that NWS is effective from the wall to $r(j)$ in the radial direction, because there are few differences in pressure in the radial direction near the centerline, as shown in Figs. 2.3(b) through 2.7(b). Hence, the volume $V(i, j)$ that NWS affects is expressed as

$$(4.2) \quad V(i, j) = \pi \left\{ (R - \Delta r)^2 - [(j-1)\Delta r]^2 \right\} \Delta x.$$

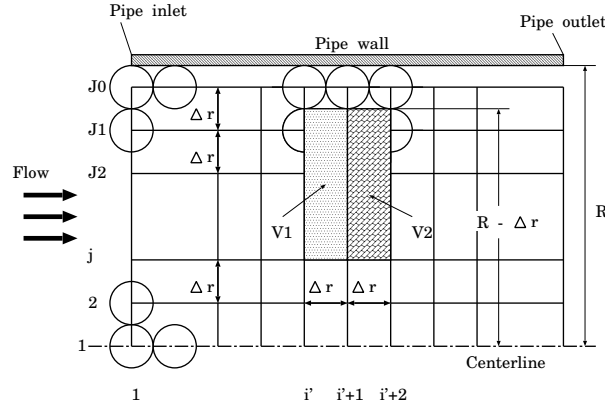


FIG. 4.1. Grid system, $\Delta x = \Delta r$.

Next, the pressure difference in the radial direction is approximated by the difference between $p(i, j)$ and $p_w(i)$:

$$(4.3) \quad \begin{aligned} \Delta p(i, j) &= p(i, j) - p_w(i) = \frac{1}{2} (p_{i,j} + p_{i+1,j}) \\ &\quad - \frac{1}{4} (p_{i,J_0} + p_{i,J_1} + p_{i+1,J_0} + p_{i+1,J_1}). \end{aligned}$$

(2) The period during which NWS acts on the flow passing along vorticities at (i, J_0) and $(i + 1, J_0)$ is considered. The distance between $x(i)$ and $x(i + 1)$ is Δx . The velocities at two points (i, J_1) and $(i + 1, J_1)$ respectively are u_{i,J_1} and u_{i+1,J_1} . Accordingly, the provisional period $\Delta t^*(i)$ may be given by dividing the axial grid space Δx by the mean velocity at $j = J_1$,

$$\Delta t^*(i) \equiv \frac{\Delta x}{\frac{1}{2}(u_{i,J_1} + u_{i+1,J_1})} \approx \frac{\Delta x}{u_{i+1/2,J_1}}.$$

However, if this provisional $\Delta t^*(i)$ is the correct period, the following inconsistency will be encountered. Two simple cases are taken as examples. First, if the grid aspect ratio is (a) $\Delta x = 2\Delta r$, as shown in Fig. 2.1, the work WK(a) and the power RW(a) for the shaded space between $x(i)$ and $x(i + 1)$ are expressed as

$$(4.4) \quad \text{WK}(a) = V \Delta p,$$

$$(4.5) \quad \text{RW}(a) = \frac{V \Delta p}{\Delta x} = \frac{(V \Delta p) u_{i+1/2,J_1}}{2\Delta r}.$$

Next, if the grid aspect ratio is (b) $\Delta x = \Delta r$ and $V_1 + V_2 = V$, as shown in Fig. 4.1, the work WK(b) in V is calculated by adding the work in V_1 and in V_2 ,

$$(4.6) \quad \text{WK}(b) = V_1 \Delta p_1 + V_2 \Delta p_2 \approx V \Delta p,$$

where it is assumed that $\Delta p_1 \approx \Delta p_2 \approx \Delta p$. Similarly, the power RW(b) in V is calculated by adding the power in V_1 and in V_2 ,

$$(4.7) \quad \text{RW}(b) = \frac{V_1 \Delta p_1}{\Delta r} + \frac{V_2 \Delta p_2}{\Delta r} \approx \frac{(V \Delta p) u_{i'+1,J_1}}{\Delta r} \approx 2\text{RW}(a),$$

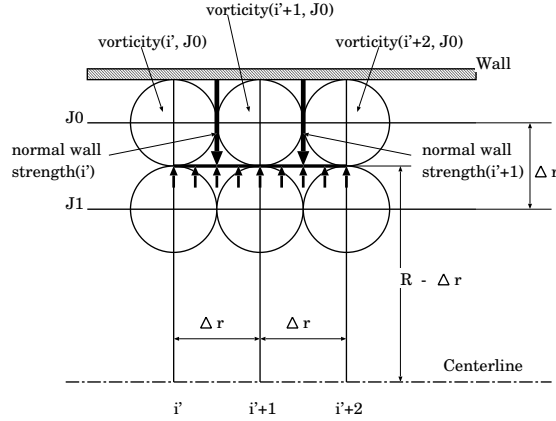


FIG. 4.2. Balance of NWS and pressure at wall.

where $u_{i'+1/2, J1} \approx u_{i'+1, J1} \approx u_{i'+3/2, J1}$. As seen from (4.4) and (4.6), WK(a) and WK(b) are the same. When comparing RW(a) and RW(b) respectively calculated using (4.5) and (4.7), however, the power RW(b) is twice as high as RW(a), although the volume and position are the same.

To avoid this inconsistency, the following period is required for a general grid system of $\Delta x = n\Delta r$ ($n = 1, 2, 3, \dots$):

$$(4.8) \quad \Delta t(i) \equiv \frac{\Delta r}{\frac{1}{2}(u_{i, J1} + u_{i+1, J1})} \approx \frac{1}{\frac{1}{2}(\omega_{i, J0} + \omega_{i+1, J0})},$$

where, from (2.12), $\omega_{i, J0} = u_{i, J1}/\Delta r$.

This period is based on the following assumptions.

(i) The no-slip condition at the wall means that the fluid particles are not undergoing translation; however, they are undergoing a rotation. It can be imagined that the wall consists of an array of marbles that are rotating but remain at the same location at the wall $j = J0$ [14].

(ii) The rotation of a fluid particle at the wall yields a vortex and vorticity. Then the curl of vorticity yields NWS from (3.3). The diameter of the vortex of the fluid particle at the wall is Δr . Accordingly, NWS is produced per vortex, or per Δr .

Figure 4.2 shows the balance between NWS and pressure at the contact surface of $j = 0.5(J0 + J1)$. For simplicity, the above statement is clarified using (3.2) and (4.9) in discrete form. Setting Δx to be $n\Delta r$,

$$(4.9) \quad \begin{aligned} \frac{\Delta p}{\Delta r} &= \frac{2}{\text{Re}} \frac{\Delta \omega}{\Delta x} = \frac{2}{\text{Re}} \frac{\omega_{i+1} - \omega_i}{\Delta x} = \frac{2}{\text{Re}} \frac{\omega_{i'+n} - \omega_{i'}}{n\Delta r} \\ &= \frac{2}{\text{Re}} \frac{1}{n\Delta r} \left[(\omega_{i'+n} - \omega_{i'+n-1}) + (\omega_{i'+n-1} - \omega_{i'+n-2}) + \dots \right. \\ &\quad \left. + (\omega_{i'+1} - \omega_{i'}) \right] \approx \frac{2}{\text{Re}} \frac{n(\omega_{i'+1} - \omega_{i'})}{n\Delta r} = \frac{2}{\text{Re}} \frac{\omega_{i'+1} - \omega_{i'}}{\Delta r}, \end{aligned}$$

where it is assumed that the vorticity gradient is linear in a small space between $x(i)$ and $x(i+1)$, i.e., $\omega_{i'+n} - \omega_{i'+n-1} \approx \omega_{i'+n-1} - \omega_{i'+n-2} \approx \dots \approx \omega_{i'+1} - \omega_{i'}$.

TABLE 4.1
 Power (RW) and evaluation criteria at $Re = 2000, J0 = 51$.

<i>No</i>	c1 $(p_c - p_w)$	c2 $(p_w - p_c)/p_c$	c3 $(p(j) - p_w)/(p_c - p_w)$	c4 ω	$X(i)$	$r(i, j)$	RW
1	0.01	–	1.00	–	0.00029	0.00	1.278
2	0.01	–	0.95	–	0.00029	0.09	1.067
3	0.01	–	0.90	–	0.00029	0.13	0.898
4	0.05	–	1.00	–	0.00016	0.00	1.085
5	0.05	–	0.95	–	0.00016	0.10	0.895
6	0.05	–	0.90	–	0.00016	0.14	0.744
7	–	0.01	1.00	–	0.00041	0.06	1.302
8	–	0.01	0.95	–	0.00041	0.16	1.089
9	–	0.01	0.90	–	0.00041	0.20	0.917
10	–	0.03	1.00	–	0.00032	0.00	1.287
11	–	0.03	0.95	–	0.00032	0.10	1.076
12	–	0.03	0.90	–	0.00032	0.13	0.906
13	–	0.05	1.00	–	0.00028	0.00	1.274
14	–	0.05	0.95	–	0.00028	0.09	1.064
15	–	0.05	0.90	–	0.00028	0.13	0.894
16	–	0.03	–	10^{-7}	0.00032	0.28	0.194

TABLE 4.2
 Power (RW) and evaluation criteria at $Re = 2000, J0 = 101$.

<i>No</i>	c1 $(p_c - p_w)$	c2 $(p_w - p_c)/p_c$	c3 $(p(j) - p_w)/(p_c - p_w)$	c4 ω	$X(i)$	$r(i, j)$	RW
17	0.01	–	1.00	–	0.00024	0.04	1.029
18	0.01	–	0.95	–	0.00024	0.13	0.814
19	0.01	–	0.90	–	0.00024	0.17	0.674
20	0.05	–	1.00	–	0.00013	0.00	0.912
21	0.05	–	0.95	–	0.00013	0.12	0.708
22	0.05	–	0.90	–	0.00013	0.17	0.579
23	–	0.01	1.00	–	0.00029	0.30	1.039
24	–	0.01	0.95	–	0.00029	0.31	0.822
25	–	0.01	0.90	–	0.00029	0.32	0.682
26	–	0.03	1.00	–	0.00026	0.08	1.035
27	–	0.03	0.95	–	0.00026	0.17	0.819
28	–	0.03	0.90	–	0.00026	0.21	0.679
29	–	0.05	1.00	–	0.00024	0.02	1.029
30	–	0.05	0.95	–	0.00024	0.13	0.814
31	–	0.05	0.90	–	0.00024	0.17	0.674
32	–	0.03	–	10^{-7}	0.00026	0.33	0.087

(3) The power $RW(i)$ for the volume $V(i, j)$ is derived from (4.2), (4.3), and (4.8). Thus the total power RW is

$$(4.10) \quad RW = \sum_i \frac{V(i, j) \Delta p(i, j)}{\Delta t(i)}.$$

4.3. Effective region of NWS. In order to calculate the power RW in (4.10), we must determine the effective axial and radial regions of NWS. The effective region is determined by the following criteria c1–c4. Here, $0 \geq p_c(i) \geq p(i, j) \geq p_w(i)$ in the radial direction.

Axially: (i) $c1 = (p_c - p_w)$, (ii) $c2 = (p_w - p_c)/p_c$.

Radially: (iii) $c3 = (p(i, j) - p_w)/(p_c - p_w)$, (iv) $c4 = \omega$.

The calculated results of RW are listed in Tables 4.1 for $J0 = 51$ and 4.2 for $J0 = 101$. The effective regions of NWS are derived using Tables 4.1 and 4.2, and Fig. 2.4 at $Re = 2000$.

TABLE 4.3
Power RW and Re.

Re	500	1000	2000	3000	5000	10,000
<i>J0</i>	RW					
51	1.562	1.327	1.076	0.910	0.692	0.420
101	1.500	1.139	0.819	0.656	0.473	0.244

(1) The axial effective length of NWS is considered. For Cases No. 4 ($c_1 = 0.05$) and 13 ($c_2 = 0.05$), the effective axial lengths are 0.00016 and 0.00028. From Fig. 2.4(a), at $X = 0.0002$, we can see a small pressure difference ($p_c - p_w$), so criterion c_2 is judged to be better than c_1 . At $X = 0.0002$, $p_c = -0.192$ and $p_w = -0.225$, $c_1 = (p_c - p_w) = 0.033$ and $c_2 = (p_w - p_c)/p_c = 0.147$. At $X = 0.0003$, we can see a very small pressure difference ($p_c - p_w$). Then, $p_c = -0.241$ and $p_w = -0.251$; $c_1 = 0.01$ and $c_2 = 0.040$. At $X = 0.0004$, there is no pressure difference ($p_c - p_w$). Then, $p_c = -0.277$ and $p_w = -0.281$; $c_1 = 0.004$ and $c_2 = 0.014$. Accordingly, the threshold of c_2 might be set at 0.030.

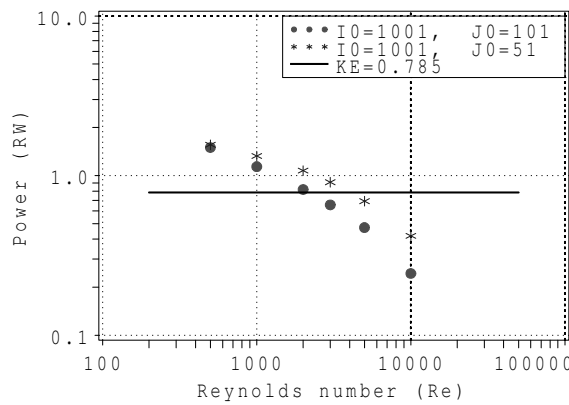


FIG. 4.3. *Power (RW) vs Re.*

(2) The radial effective length is considered. For Cases No. 23 and 26 ($c_3 = 1.00$) in Table 4.2, the pressure is constant from $r = 0$ (centerline) to $r = 0.30$ and from $r = 0$ to $r = 0.08$, respectively. For Cases No. 23 through 25, $c_3 = 1.00$ at $r = 0.30$, 0.95 at $r = 0.31$, and 0.90 at $r = 0.32$, respectively. Accordingly, the threshold of c_3 might be set at 0.95.

(3) The vorticity is transferred from near the wall into the central core by NWS. For Cases No. 16 and 32, the penetrated radial length of $\omega = 10^{-7}$ is $r = 0.28$ for $J_0 = 51$ and 0.33 for $J_0 = 101$. Since the value of RW is very small, such as 0.194 and 0.087, respectively, we cannot use c_4 as a criterion for determining the effective region of NWS.

4.4. Calculation of minimum R_c . The calculated RW values are listed in Table 4.3 and plotted against Re in Fig. 4.3, where the asterisks and dots denote the calculated results for $J_0 = 51$ and $J_0 = 101$, respectively.

The minimum critical Reynolds number $R_c(min)$ is calculated via linear interpolation employing the values of RW for $Re = 2000$ and 3000 ,

$$\frac{R_c(min) - 3000}{2000 - 3000} RW \Big|_{Re=2000} + \frac{R_c(min) - 2000}{3000 - 2000} RW \Big|_{Re=3000} = 0.785.$$

We thus obtained $R_c(\min)$ of 3750 when $J_0 = 51$ and 2200 when $J_0 = 101$.

Conclusions. A conceptual macromodel was built to determine $R_c(\min)$ for pipe flows, on the basis of the results of our experiments and previous calculations. The calculated results were $R_c(\min) = 3750$ when $J_0 = 51$ and 2200 when $J_0 = 101$.

The model is based on NWS. NWS causes the difference ($p_c - p_w$) in the radial direction and accelerates fluid particles in the central core. In the entrance region, the velocity profile changes from a uniform distribution at the pipe inlet to a parabolic one in the fully developed region. The fluid particles in the central core are accelerated. The magnitude of the required nondimensional acceleration power is $KE = 0.785$, which is derived from the difference in kinetic energy between the flow at the inlet and that in the fully developed region.

The occurrence of the transition depends on the acceleration power RW given by NWS:

- (a) when $RW < 0.785$, transition takes place;
- (b) when $RW \geq 0.785$, transition never takes place.

A detailed study of the physical mechanism behind NWS and the occurrence of transition will be a future work.

Acknowledgment. We wish to express our sincere appreciation to Emeritus Professor F. Stenger of the University of Utah, Professor T. K. DeLillo of Wichita State University, and Dr. K. Shimomukai of SGI Japan for useful advice and encouragement, and to the Information Synergy Center, Tohoku University, for its outstanding computational services.

REFERENCES

- [1] R.-Y. CHEN, *Flow in the entrance region at low Reynolds numbers*, J. Fluids Eng., 95 (1973), pp. 153–158.
- [2] P. G. DRAZIN AND W. H. REID, *Hydrodynamic Stability*, Cambridge University Press, 1981, p. 219.
- [3] S. GOLDSTEIN, *Modern Developments in Fluid Dynamics, Vol. 1*, Dover, 1965, pp. 97, 297–309.
- [4] R. A. GRANGER, *Fluid Mechanics*, Dover, 1995, pp. 481–484.
- [5] L. M. HUANG AND T. S. CHEN, *Stability of the developing laminar pipe flow*, Phys. Fluids, 17 (1974), pp. 245–247.
- [6] L. M. HUANG AND T. S. CHEN, *Stability of developing pipe flow subjected to non-axisymmetric disturbances*, J. Fluid Mech., 63 (1974), pp. 183–193.
- [7] H. KANDA, *Numerical study of the entrance flow and its transition in a circular pipe*, ISAS (Institute of Space and Astronautical Science), Tokyo, Report No. 626, 1988.
- [8] H. KANDA, *Computerized model of transition in circular pipe flows. Part 2. Calculation of the minimum critical Reynolds number*, ASME (American Society of Mechanical Engineers) FED, 250 (1999), pp. 197–204.
- [9] H. KANDA, *Laminar-turbulent transition: Calculation of minimum critical Reynolds number in channel flow*, RIMS (Research Institute for Mathematical Science, Kyoto Univ.) Kokyuroku, Bessatsu B1, 2007, pp. 199–217.
- [10] H. KANDA AND T. YANAGIYA, *Hysteresis curve in reproduction of Reynolds's color-band experiments*, J. Fluids Eng., 130 (2008), 051202 (10 pages).
- [11] R. R. KERSWELL, *Recent progress in understanding the transition to turbulence in a pipe*, Nonlinearity, 18 (2005), pp. R17–R44.
- [12] D. KONDEPUDI AND I. PRIGOGINE, *Modern Thermodynamics*, John Wiley & Sons, 1998, pp. 22, 55–56.
- [13] M. J. LIGHTHILL, *Laminar Boundary Layers*, L. Rosenhead, ed., Dover, 1988, p. 54.
- [14] R. L. PANTON, *Incompressible Flow*, Wiley-Interscience, 1984, p. 323.
- [15] P. J. ROACHE, *Fundamentals of Computational Fluid Dynamics*, Hermosa, 1998, pp. 196–200.
- [16] O. REYNOLDS, *An experimental investigation of the circumstances which determine whether the motion of water shall be direct or sinuous, and of the Law of resistance in parallel channels*, Trans. Royal Soc. London, 174 (1883), pp. 935–982.
- [17] A. H. SHAPIRO, R. SIEGEL, AND S. J. KLINE, *Friction factor in the laminar entry region of a smooth tube*, Proc. 2nd Natl. Congr. Appl. Mech., ASME, 1954, pp. 733–741.
- [18] K. SHIMOMUKAI AND H. KANDA, *Numerical study of normal pressure distribution in entrance flow between parallel plates. I. Finite difference calculations*, Electron. Trans. Numer. Anal., 23 (2006), pp. 202–218. <http://etna.math.kent.edu/vol.23.2006/pp202-218.dir/pp202-218.html>.

- [19] K. SHIMOMUKAI AND H. KANDA, *Numerical study of normal pressure distribution in entrance pipe flow*, Electron. Trans. Numer. Anal., 30 (2008), pp. 10–25.
<http://etna.math.kent.edu/vol.30.2008/pp10-25.dir/pp10-25.html>.
- [20] S. TANAKODA, *Fluid Dynamics by Learning from Flow Images (in Japanese)*, Asakura Publishing Co., Tokyo, 1993, p. 165.
- [21] T. TATSUMI, *Stability of the laminar inlet-flow prior to the formation of Poiseuille regime*, J. Phy. Soc. of Japan, 7 (1952), pp. 489–502.

Appendix A.

A.1. Nomenclature.

C_b	=	contraction ratio = D_b/D
D	=	pipe diameter = $2R$
D_b	=	bellmouth diameter
H	=	enthalpy = $U + pV$, where V is volume
i	=	axial point of grid system
$I0$	=	number of axial grid points
j	=	radial point of grid system
$J0$	=	number of radial grid points
KE	=	increase in kinetic energy (unit is power); see (3.6)
NWS	=	normal wall strength; see (3.3)
p	=	pressure = $p'/((1/2)\rho U_0^2)$
r	=	radial coordinate = r'/D
R	=	pipe radius = $R'/D = 0.5$
Re	=	Reynolds number = $U_0 D/\nu$
RW	=	power done by NWS or rate of change of work; see (4.10)
t	=	time = $(U_0/D)t'$
T	=	temperature
u	=	axial velocity
U_0	=	mean axial velocity at pipe inlet
U	=	internal energy
v	=	radial velocity
V	=	velocity vector or volume
WK	=	work done by NWS
x	=	axial coordinate = x'/D
x'	=	actual axial coordinate
X	=	axial coordinate = $x/Re = x'/(DRe)$
ρ	=	fluid density
ψ	=	streamfunction = $\psi'/(U_0 D^2)$
ω	=	vorticity = $(D/U_0)\omega'$
θ	=	angle in cylindrical coordinates
ν	=	kinematic viscosity
Δp	=	pressure drop
Δr	=	radial grid size
Δx	=	axial grid size

Superscript: (') = dimensional quantity

A.2. Flowchart for explicit iteration method.

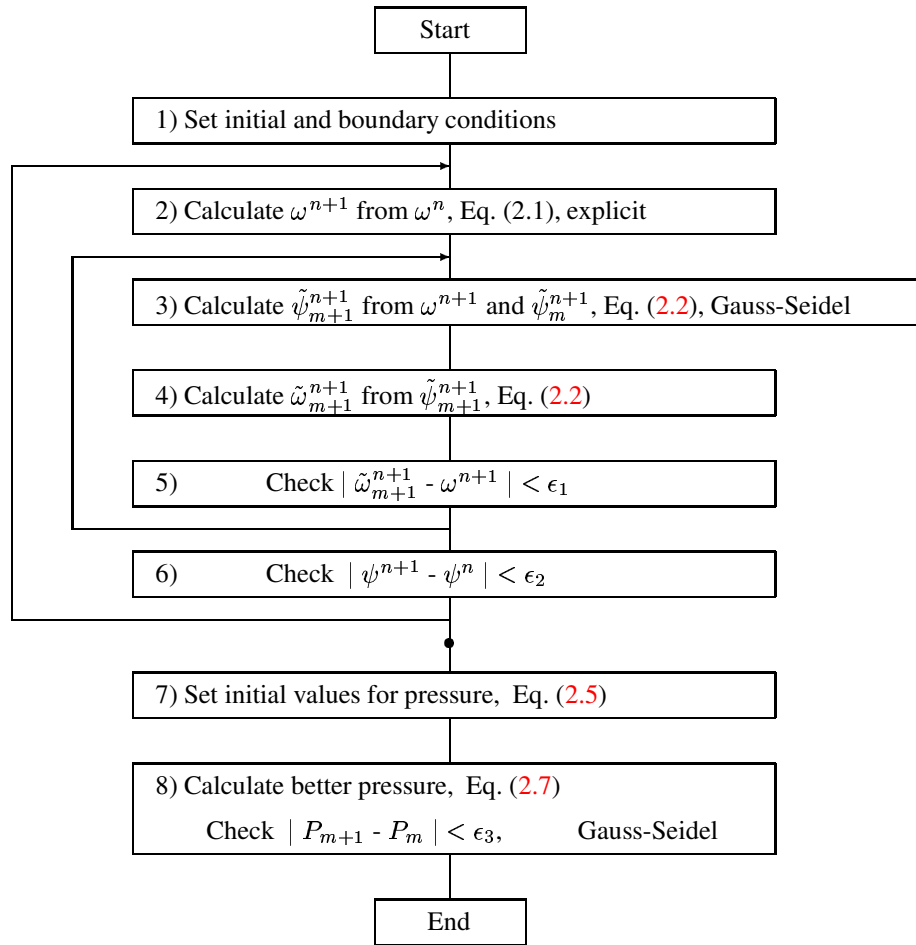


FIG. A.1. Flowchart for explicit iteration method.